Fluorescence Recovery after Photobleaching as a Probe of Diffusion in Starch Systems

Paul A. Perry,[†] Melissa A. Fitzgerald,[‡,§] and Robert G. Gilbert*[,†]

NSW Department of Primary Industries, Yanco Agricultural Institute, PMB Yanco, NSW 2703 Australia, Key Centre for Polymer Colloids, School of Chemistry F11, University of Sydney, NSW 2006 Australia, Yanco Agricultural Institute, PMB, Yanco, NSW 2703 Australia, and International Rice Research Institute, DAPO Box 7777, Metro Manila, The Philippines

Received October 16, 2005; Revised Manuscript Received December 5, 2005

The diffusion coefficients of dextran probes of various molecular weights in starch solutions over a wide concentration range were carried out using fluorescent recovery after photobleaching (FRAP), combined with a confocal microscope and tracer probe diffusion. The technique is simple to implement and can be carried out using increasingly common microscopy apparatus, giving access to a wide variety of new structural and kinetic information. The data can be rationalized in terms of the effects of probe molecular weight and on matrix starch concentration and structure. This provides a new tool to investigate the behavior of systems where starch is an ingredient that contributes to the processing and textural properties of food.

Introduction

Starch is composed of two high molecular weight polymers of glucose: linear amylose and the highly nonrandomly branched and semicrystalline amylopectin. The most commonly encountered physical form of starch when in conventional use is the gelatinized starch paste, which is made up of disrupted granules in a matrix of amylose and amylopectin that gels and eventually retrogrades and crystallizes upon storage. One of the main factors preventing the more widespread advance in the uses of unmodified starch is the lack of a clear understanding of the relationship between molecular structure and diffusion of these often highly complex, multicomponent, branched, and highly entangled systems that we find in a gel or solution of gelatinized starch. Conventionally, flow and diffusion properties are measured in bulk systems (e.g., by rheometry or rapid visco-analysis) or using highly diluted samples (e.g., by photon correlation spectroscopy). These properties are then traditionally interpreted in terms of microstructure and molecular structure/architecture, determined using alternative techniques. In all cases, diffusion of the constituent polymer chains and the resulting system viscosity (and especially the way in which this changes as the result of various processing techniques or physical transformations/storage conditions) and the diffusion of smaller trace components and added material (sugars, flavor compounds, enzymes, etc.) are of great significance with regard to the material properties of the starch. The diffusion coefficient of species of various sizes is important for many food-related properties: for example, the texture of processed foods in which starch is an ingredient of the matrix, such as the low-fat products where sugar is replaced with starch and dextrans (e.g., yoghurt, baby food, pie-fillings, and pastry fillings). Rheological data such as from RVA tend to be strongly influenced by longer chains and so cannot be used to make inferences on diffusion of small species.

In recent times, a range of optical-microscopy-based techniques have emerged that allow one to probe the diffusion and viscosity characteristics of both simple and highly complex concentrated systems, nondestructively and with simultaneous imaging of the microstructure. One of the most versatile and simple of these techniques is fluorescence recovery after photobleaching (FRAP) which when combined with a confocal laser scanning microscope (CLSM) opens up whole new avenues of investigation in the area of structure−dynamics relationships on the local, micron-scale level. The spatial resolution, in all three dimensions, of the confocal-FRAP technique also offers the potential to map systems or to measure inhomogeneities within a single bulk sample.[1]

FRAP is one of a family of photobleaching techniques for the measurement of diffusion coefficients of fluorescently tagged molecules and dyes. Other methods include fluorescence loss in photobleaching (FLIP), inverse FRAP (iFRAP),[2−4] fringe pattern photobleaching, and forced Rayleigh scattering (FRS).[5−7] In each case, a concentration grating pattern or region of interest (spot, line, or geometric shape) is photobleached in a sample containing fluorescently tagged molecules of interest using a high powered laser. This involves subjecting the fluorescent molecules to a very high-intensity pulse of radiation at the excitation wavelength, which renders the fluorophore unable to fluoresce. This is the "writing" step. Following photobleaching, the "reading" step involves monitoring the time course of the return to equilibrium of the fluorescent levels within the particular region of interest.

The method of FRAP was initially designed by Axelrod and co-workers[8] to measure two-dimensional diffusion of membrane-bound molecules. It uses the phenomenon of irreversible photobleaching of fluorescent probes to measure parameters related to molecule mobility. Frequently, photobleaching interferes with image acquisition in fluorescence microscopy by fading the fluorescent probes, resulting in a lower signal/noise ratio. However, in FRAP experiments, this phenomenon is used to selectively photobleach a specific area in a sample, throughout

* To whom correspondence should be addressed. Author address: Key Centre for Polymer Colloids, School of Chemistry F11, University of Sydney, NSW 2006 Australia. Fax: +61 2 9351 8651. E-mail: gilbert@chem.usyd.edu.au.

[†] University of Sydney.

[‡] International Rice Research Institute.

[§] NSW Department of Primary Industries.

10.1021/bm0507711 CCC: $33.50
Published on Web 01/11/2006

which the fluorophores are homogeneously distributed, using a high intensity laser. Subsequently, the kinetics of fluorescence recovery, brought about by diffusion/flow of nonbleached fluorescent species back into the region of interest, are recorded by sampling images at regular time intervals using the same, but highly attenuated, laser beam. This is accompanied by diffusion of bleached molecules out of the region of interest into the unbleached surrounding matrix, but this generally results in only a slight decrease in fluorescent intensity in the area surrounding the bleach that is often very difficult to detect. FLIP on the other hand uses the loss of fluorescence from the region surrounding a bleach zone as its main principle of operation. Values of molecular mobility and viscosity can be determined directly from the rate of fluorescence recovery; diffusion coefficients can be obtained from the rate of recovery and the geometry and depth of the bleached region, in systems where diffusion is the only transport mechanism. When combined with a confocal microscope, FRAP is capable of probing mobility within specific volume elements of a sample, rather than in the bulk, hence the utility in systems in which there is spatial heterogeneity. Latex particles and fluorescently labeled dextran polymers are the most commonly used probes in nonbiological applications.

Characteristic recovery times are typically determined from fitting a variety of algorithms to the experimental data using nonlinear least squares regression. Direct determination of the half time for recovery is also possible, where we have a good estimate of the total fractional recovery at a long time (typically $\sim 25t_{1/2}$, where $t_{1/2}$ is the half-life) after bleaching. Many methods have been employed to fit to the form of the recovery curves, including biexponential, series expansions and more empirical determinations. In all cases, it is found that the shape of the curve is the same in all cases where diffusion (as opposed to directed flow or other modes of transport) is the only source of fluorescence recovery, with a single time parameter being sufficient to characterize differences in recovery rate.

Here we report the first application of FRAP to the study of diffusion of probe molecules in gelatinized starch.

Experimental Section

Materials and Methods. Fluorescein isothiocyanate conjugate tagged dextrans (FITC-dextran) of two different weight average molecular weights ($\bar{M}_w = 7.0 \times 10^4$ and 2.5×10^5, denoted FD70S and FD250S) were obtained from Sigma Chemical Co. and used as received. Both contained 0.003−0.02 mol of FITC per mol of glucose and had stated polydispersities ($\bar{M}_w/\bar{M}_n$) < 1.30. Glycerol (99+%) and 2.0×10^6 $\bar{M}_w$ dextran (D5376) were also obtained from Sigma. FITC-dextrans were chosen as the probes due to the excitation and emission of FITC (~488 nm/512 nm) being ideally suited to the argon ion laser of the confocal microscope and also because FITC-dextrans are commercially available in a range of molecular weights. The hydrodynamic radius of the 7.0×10^4 probe was quoted to be 6 nm by the supplier, a value supported by other experimental studies.[9,10] The radius of the 2.5×10^5 $\bar{M}_w$ probe was calculated to be ~10.2 nm, from the zero-concentration diffusion coefficients of the two probes using the Stokes Einstein relationship.

Three starch varieties were investigated: Shimizu Mochi, a commercial waxy rice, Amioca starch, from waxy Maize, and Stakote 7, a partially acid-hydrolyzed derivative of Amioca. The latter two were obtained from National Starch and Chemical Company and were used as received. Shimizu Mochi was received as flour obtained from grinding milled rice to pass through a 0.5 mm sieve (Cyclotec 1093 sample mill, Tecator, Hoganas, Sweden). Starch was obtained from this Shimizu Mochi flour by Soxhlet extraction of lipids and protease treatment to remove proteins, according to the methods of Chiou et al.[11]

Starch solutions were prepared in a Siltex 175D autoclave, using the "gentle" 121 °C cycle, with 0.01 M acetic acid (pH 3.5) as the solvent. Solutions were subsequently neutralized (to between pH 7 and 8) using 0.1 M NaOH, and the final concentration of starch was determined by gravimetry. Starch solution concentrations ranged from highly dilute to the limit of acceptable solubility (a range of ~ 0.1%−15% w/w in all cases). Dextran solutions were prepared in water, with gentle heating (maximum 60 °C) and stirring. Fresh solutions of fluorescent probe were mixed with the cooled starch solutions, before depositing in dimpled double concave microscope slides (26 × 76 mm, Bacto Laboratories, NSW, Australia) with a glass cover slide, sealed with nail-varnish.

Aqueous-phase size-exclusion chromatography (SEC) was carried out using a system comprising a Shimadzu inline degasser, Shimadzu pump, a Shimadzu autoinjector, and a Shimadzu system control unit. Separation was carried out using a Waters Ultrahydrogel 500 column and detection was with a Wyatt Optilab DSP interferometric refractometer, controlled and recorded by a computer running Astra software. The eluent was ammonium acetate buffer (0.05M, pH 5.2). The flow rate was 1 mL min^{-1} and the total run time was 30 min.

FRAP Protocol. FRAP experiments were carried out using a Leica TCS SPII multiphoton inverted confocal microscope using a Leica 10× dry PL Fluotar objective lens, with a quoted numerical aperture of 0.3; however, with the beam expander removed and the image not completely filling the back focal plane, the effective numerical aperture was 0.1. The 10× objective lens was chosen to have a cylindrical bleaching volume, enabling diffusion in the third dimension to be avoided. Further reasons for use of such a low numerical aperture lens are included in the section on data analysis. Samples were contained within a dimpled glass slide and were then sealed with a glass cover slide.

For all solution data, where absolute diffusion coefficients are determined, a uniform disk bleach of radius ~36 μm was used, with the microscope zooming to bleach.

Samples were bleached for between 0.5 and 1.1 s using 100% power from a 25 mW argon ion laser. Bleaching times and the time of capture of each recovery frame could be altered in two major ways: increasing the scan speed of the laser and reducing the resolution (number of lines scanned by the laser in each frame). Increasing scan speeds resulted in a significant "bleach tail", where the laser did not cut off precisely at the edge of the prescribed bleach region, leading to a nonuniform circular bleach. Reducing the number of lines scanned, from 512 × 512 to 256 × 256, and even 128 × 128 in some cases, proved to be a much more efficient means of reducing bleach times and was the method used in all experimental runs presented here. Post-bleach recovery images and the initial pre-bleach baseline were recorded using between 2 and 4% of the full laser power, depending on the intensity of fluorescence from the sample. Unless otherwise stated, recovery images were collected using a fully open aperture (600 μm), at a zoom setting of 2. In all cases, bleaching and monitoring of recovery were performed at a depth of 50−100 μm within the sample (above the inner cover slide surface, as we are using an inverted microscope). At this depth of the focal and bleach plane signal-to-noise ratio was maximized while any possible boundary effects were avoided. However, despite slight variations in data quality, over a depth range of approximately 10−225 μm, there was found to be no effect of depth on the recovery times or diffusion coefficients measured.

Data were collected as a series of image frames, captured at regular intervals prior to and after the single bleach frame. The time between frames, as with the bleach frame, was determined by the area of the scan, the scan speed, and the number of lines per scan and ranges between 0.5 and 1.1 s. Fluorescent intensity was measured from the volume and position of the original bleach and in the same size and shape volume element from another, physically unaffected region of

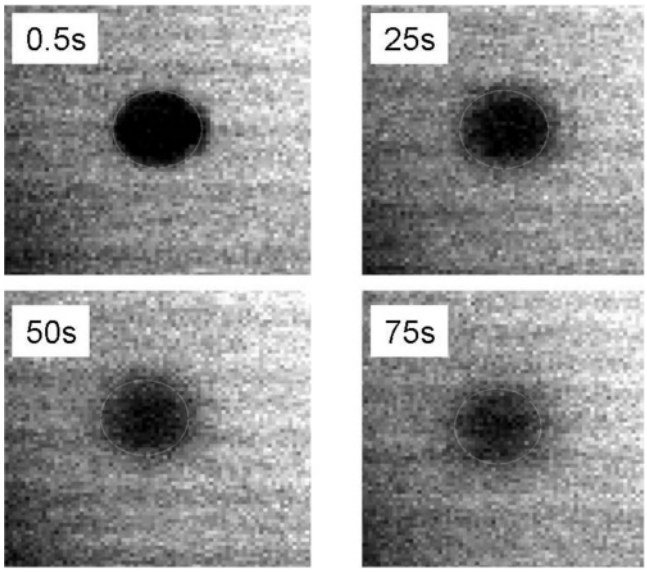

Figure 1. Images showing recovery of fluorescent intensity within the bleach disk. The circle enclosing the lower intensity region marks the area of intensity integration.

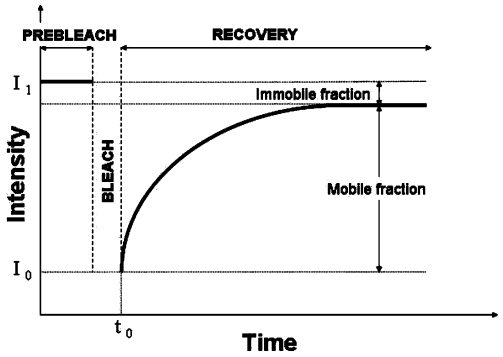

Figure 2. Schematic of a FRAP recovery curve. I_1 and I_0 represent the pre-bleach and the immediate post-bleach intensities, respectively, and t_0 represents the zero point time of recovery.

the image frame, as a background. Figure 1 shows the general form that the recovery takes in images taken at 25 s intervals following the single frame uniform disk shaped bleach. The circles traced onto these images mark the 2D size and position of the original bleach disk and indicate the lateral area over which the changing fluorescent intensity is measured during the recovery phase. This particular example was for the bleaching of a 70% glycerol (w/w) solution mixed with 2 mg mL^{-1} 7.0×10^4 M_w FITC-dextran probe. The radius of the bleach disk was 36 μm.

Any drift of the bleach disk was immediately apparent from the raw data, as illustrated in Figure 1. Any drift was also revealed by tracking of the center of the mass of the bleached area; any experimental runs displaying drift were discarded.

The general form of the recovery curve and its main features are illustrated in Figure 2. Raw recovery curves were produced from plotting the variation in integrated intensity within the bleach disk volume as a function of time. The final recovery curve was obtained by subtracting a background, obtained by scanning an equivalent size in a region well away from the influence of photobleaching. This subtraction thus takes into account any variation of the laser intensity and any bleaching of the sample that takes place during the collection of recovery phase information. This treatment was followed by normalization using the pre-bleach fluorescent intensity.

In the absence of any flow or directed transport, where diffusion is the only transport mechanism for fluorophores within the system, all recovery curves have the same shape, with the time axis being the only variable parameter.

All normalized recovery curves can be overlaid by suitable scaling of the time axis. As pointed out by a referee, this is a consequence of a "top hat" bleach pattern, and does not hold for Gaussian hole bleaching, as in the original Axelrod work.[8]

Data Analysis. Normalized recovery curves were analyzed by two separate methods, both of which give absolute values of two-dimensional lateral diffusion coefficients corresponding to the three-dimensional system.

The most popular model used to determine the absolute lateral diffusion coefficient from experimental FRAP data is the 2D Gaussian spot diffusion model of Blonk.[12] Although this theory is only strictly applicable to situations in which bleaching is carried out with a *stationary* beam having a Gaussian spot geometry, it has been applied to a range of situations where bleaching is of varied geometry, such as circular, line, and even square bleaches[1,13] and where a *scanning* beam is used. In this model, the normalized recovery curve is represented by the series expansion

$$F(t) = \sum_{n=0}^{\infty} \frac{-\kappa^n}{n!} \frac{1}{1 + n\left[1 + \left(\frac{2t}{\tau_r}\right)\right]} \quad (1)$$

where κ is a bleach depth parameter and τ_r is the characteristic recovery time, which in turn is defined as

$$\tau_r = \frac{\omega^2}{4D} \quad (2)$$

where D is the 2D lateral diffusion coefficient and ω is the e^{-2} radius of the Gaussian bleach spot.

In practice, this model was applied in this work to recovery data from the bleaching of a uniform disk, with uniform bleaching of fluorescence intensity across the radius, except at the edges of the bleach region. The radius of the disk was taken as the value of ω. It was also found that values returned by the model converged after only 7 terms in the series, making expansion beyond this level unnecessary and greatly simplifying the data fitting. Data were fitted using this stationary diffusion model using the nonlinear least squares regression package in the Origin graphing and data analysis package; the fitting parameters are κ and τ_r.

Recently, a much more rigorous 3D method, specifically derived from the method of operation of the confocal microscope using a *scanning* beam has been developed by Braeckmans et al.[14] There has been little application of this method to this point. In this paper, we model data using the method of Braeckmans. Absolute diffusion coefficients derived from this model are also compared with the values given by the Gaussian spot model.

In the model of Braeckmans, the normalized recovery curve is given by

$$\frac{F_{tot}(t)}{F_0} = 1 + \sum_{n=1}^{\infty}\left[\frac{(-K_0)^n}{n!}\frac{1}{\sqrt{1+n}}\right][1 - e^{-2(\tau_r/t)}][I_0(2\,\tau_r/t) + I_1(2\,\tau_r/t)] \quad (3)$$

where τ_r is the characteristic recovery time, I_0 and I_1 are the modified Bessel functions of the zero and first order, respectively, and K_0 is the bleaching parameter (a function of the zoom setting, the line scanning speed and the interline distance of the microscope, and the bleach rate, which depends on the fluorophore and medium and the intensity distribution of the bleaching beam). K_0 is fitted, noting that its value is constant for a given set of runs.

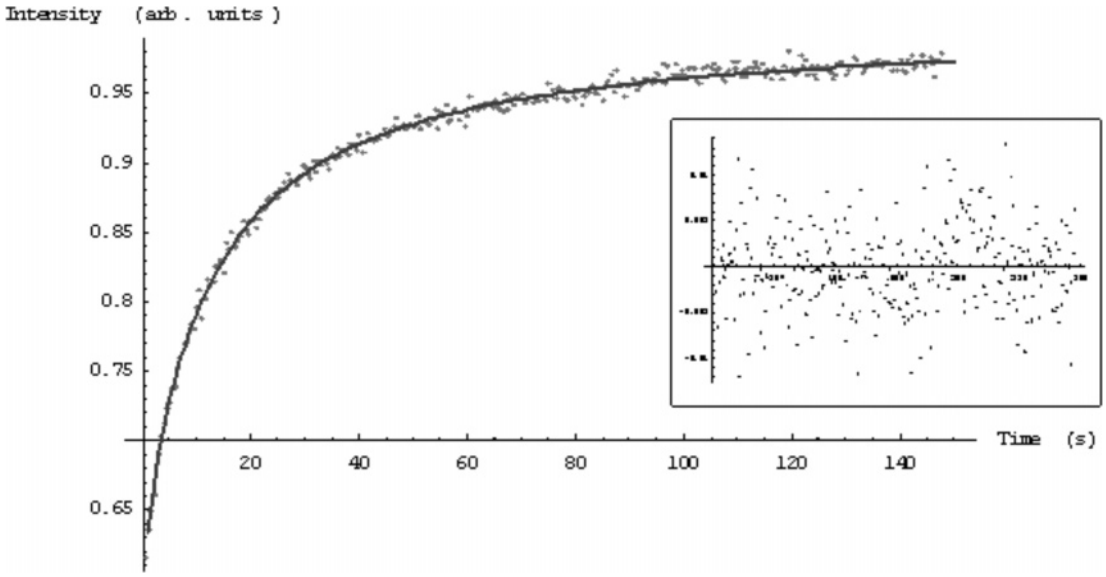

Figure 3. Example of fitting (solid line) of Braeckmans' model[14] to data from a dilute rice starch solution. Inset figure shows the residuals for the fit to the experimental data.

To take account of fractional recovery, the right-hand side of the recovery equation is substituted into

$$\frac{F_{tot}(t)}{F_0} = 1 + k\left(\frac{F_{tot}(t)}{F_0} - 1\right) \quad (4)$$

where k is the mobile fraction.

Provided an objective lens of low numerical aperture is used for bleaching and observation (this requirement can be removed if the sample is thin compared to the axial resolution of the scanning beam) and a fully open confocal aperture is used, the complicated problem of 3D diffusion reduces down to the far simpler case of 2D lateral diffusion for a uniform disk bleached by a stationary beam. The lateral 2D diffusion coefficient, D, is then given by eqs 1 and 2 but with ω in this case explicitly defined as the radius of the uniform bleach disk.

Low numerical aperture in this case means ~0.2. The experimental setup used in this work satisfies this requirement. There are a number of other conditions that must be met by any FRAP experiment, namely: uniform distribution of fluorophore, short bleaching times compared to the recovery time (a rule of thumb is at least 15× smaller than the characteristic recovery time[13]), and the absence of any flow in the sample or boundary conditions within the area of interest.

FRAP data were fitted using this full diffusion model for a uniform disk bleach geometry using the Mathematica software package. An example of the form of the experimental data, and the model fit to these data (including residuals) is shown in Figure 3. Where data were not well fitted by this full expression, there was always accompanying evidence that directed flow due to air bubbles or convection currents acted to accelerate the apparent recovery due to drift of the bleach spot.

Results and Discussion

Recovery Times and Calibration. Figure 4 compares the free diffusion coefficient (at a concentration of 2 mg mL^{-1} in water) of the 7.0×10^4 $\bar{M}_w$ FITC-dextran probe determined using the current FRAP setup and the confocal diffusion model as presented by Braeckmans et al. (eq 3) in relation to values of other molecular weight dextrans determined from studies using both FRAP[15]and NMR.[16,17] Note that the NMR values of Callaghan et al.[16] were obtained with un-tagged dextrans, rather than their fluorescent derivatives; this is not expected to affect the diffusion coefficient significantly. The molecular weight dependence of the infinite-dilution diffusion coefficient of FITC-dextran determined in this work using the scanning beam model[14] ($D \sim \bar{M}_w^{-0.52\pm0.05}$) fits well with other values in the literature[18] and is in agreement with Flory's scaling law for a linear or randomly branched chain in a good solvent at infinite dilution.[19] This law predicts a power law exponent ranging from 0.5 for a theta solvent to 0.6 for a good solvent. A branched polymer will have a maximum value of the exponent of less than 0.6, since even in a very good solvent it cannot be as highly extended as a linear polymer.

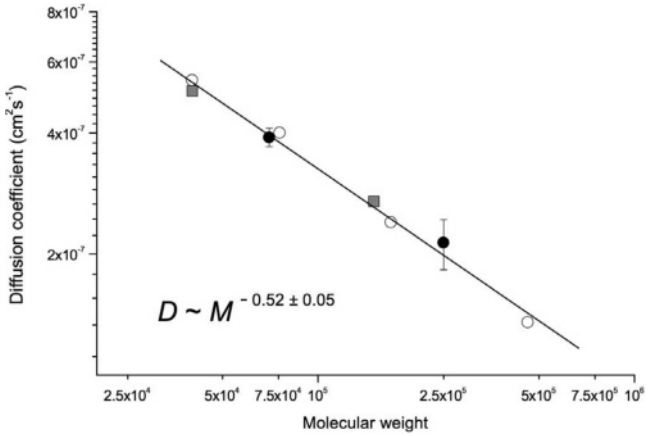

Figure 4. Comparison of the FRAP-determined free diffusion coefficient from the current work with literature values for a range of molecular weight dextrans. Current FRAP data (filled circles), FRAP data of Furukawa (filled squares)[15] and Callaghan PFG-NMR data (open circles).[16,17]

Fitting Raw FRAP Data. In systems with the most rapid diffusion, where we are monitoring probe diffusion at infinite dilution in water or in very dilute biopolymer solutions, the Braeckmans model returns values of the free diffusion coefficient that match very well with values quoted in the literature and those which are calculated form simple molecular weight scaling relationships (see Recovery Times section). This is despite the fact that in the majority of these cases we are not strictly operating under ideal conditions, with the characteristic recovery time (~7.5−8.5 s) being less than the "ideal" ~15× greater than the bleach time (~0.5−1.1 s). The Gaussian model is less tolerant in this regime, often generating values of the diffusion coefficient that are significantly lower than expected.

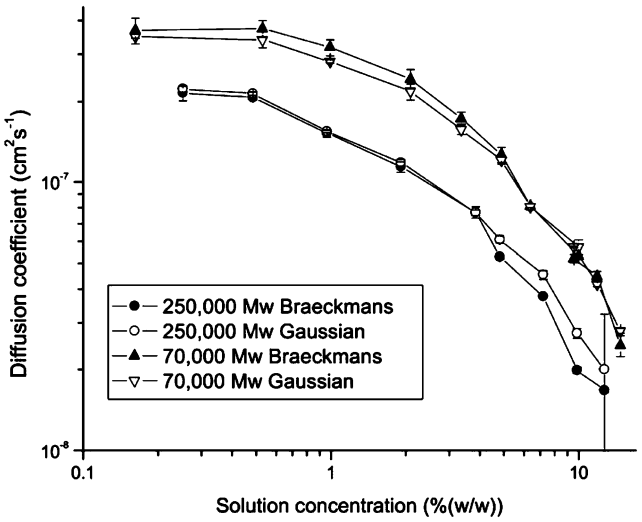

Figure 5. Variation in diffusion coefficient obtained from FRAP data using two different models for two different molecular weight probes in solutions of varying concentrations of the same polymer (2×10^6 $\bar{M}_w$ dextran). Lines joining data points are only as a visual guide.

Due to restrictions on the lower limit of the bleach time possible using the confocal setup used here, it was not possible to test the link between the calculated diffusion coefficient and the lower limit of the ratio of bleach time:recovery time. However, in all cases where data were collected in the "ideal" time regime, both methods returned very similar values of the lateral diffusion coefficient, to within the limits of the experimental error. Figure 5 shows the values of the absolute diffusion coefficients obtained from fitting FRAP data from a 2×10^6 molecular weight dextran at a range of concentrations, using tracer probe molecules of $\bar{M}_w = 7.0 \times 10^4$ (radius of gyration $\langle s^2 \rangle^{1/2} = 6$ nm calculated from the Stokes−Einstein relationship and the observed diffusion coefficient at low concentration) and $\bar{M}_w = 2.5 \times 10^5$ ($\langle s^2 \rangle^{1/2} = 10.2$ nm) FITC-dextrans, using the stationary Gaussian beam expression, eq 1, and the scanning beam model of Braeckmans, eq 3. The variation of the diffusion coefficient with increasing polymer concentration is dealt with in detail in the next section.

The consistency of the two models is reassuring, given the widespread use of the Gaussian stationary beam expression to model experimental FRAP data from diverse bleach geometries and from experimental setups that use a scanning beam. The major advantage of the Braeckmans model lies in its robustness under nonideal conditions as well as its ability to highlight "erroneous" data. The Blonk Gaussian beam model was found to be capable of fitting equally well almost any data set, even where there was pronounced drift of the bleach spot. In these cases, separate examination of image files was necessary to eliminate data from experiments in which significant drift occurred. As pointed out by a referee, an intense Gaussian profile can resemble a top-hat profile because the high intensities will be "shaved off" by fluorophore depletion. The Braeckmans model on the other hand only provided a satisfactory fit to the experimental recovery data for experimental runs where no bleach drift was present. Any drift of the bleach spot resulted in recovery curves that could not be modeled well by the Braeckmans expression, as recovery now was driven not only by diffusion but by directed flow as well. Any deviation from pure diffusion behavior was clear from the inability of the Braeckmans model to fit the data satisfactorily. For these reasons, all values quoted in this work are derived from modeling the recovery curve using the method of Braeckmans.

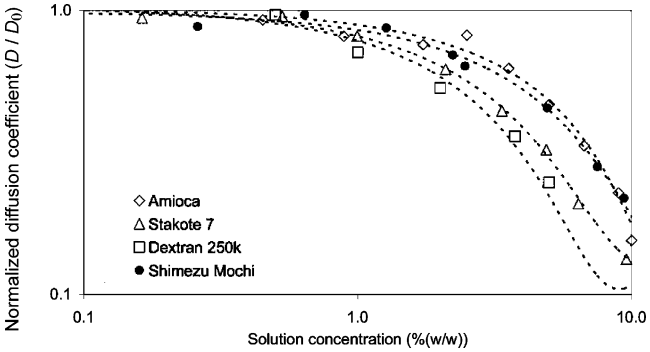

Figure 6. Dependence on matrix starch concentration of reduced diffusion coefficient D/D_0, where D_0 is the zero-concentration limiting value.

Table 1. Parameters from Stretched Exponential Fits of Diffusion Coefficient as a Function of Concentration for Various Starches

matrix starch	probe $\bar{M}_w$	$D_0/10^7$ cm^2 s^{-1}	β	υ
Shimizu Mochi	7.0×10^4	3.5 ± 0.1	0.14 ± 0.04	1.1 ± 0.1
Amioca	7.0×10^4	3.7 ± 0.1	0.12 ± 0.04	1.1 ± 0.1
Stakote7	7.0×10^4	3.9 ± 0.5	0.17 ± 0.09	1.0 ± 0.2
2×10^6 $\bar{M}_w$ dextran	7.0×10^4	3.9 ± 0.1	0.23 ± 0.03	0.93 ± 0.07
2×10^6 $\bar{M}_w$ dextran	2.5×10^5	2.3 ± 0.2	0.43 ± 0.06	0.77 ± 0.06

Diffusion Coefficients in Starch Solutions. The solution properties, and most particularly the viscosity, of polymers are clear indicators of the size and structure of the constituent chains. The magnitude of the increase in viscosity due to increasing starch concentration is related inter alia to the dimensions of the starch polymer molecules in solution. Determination of fundamental properties of dilute solutions of starch varieties grants us an insight into the behavior and interactions of the starch chains and should allow us to predict elements of the behavior at higher concentrations and in real applications.

The simplest comparison of diffusion data for the various starches is through examination of the concentration dependence of the reduced diffusion coefficient D/D_0, where D_0 is the diffusion coefficient in the limit of zero starch concentration. Table 1 gives the values of D_0 for the various matrix starches, and the reduced diffusion coefficient data are shown in Figure 6.

These matrix starches are qualitatively different in structure. Figure 7 gives SEC chromatograms that shows the increased relative amount of chains of low hydrodynamic volumes (which elute at long retention times) present in Stakote 7, as opposed to its native, untreated parent, Amioca. It is essential to recall at this point that SEC separates on polymer size (hydrodynamic volume), which does not correspond directly to molecular weight in the case of branched polymers such as those used here. However, because Stakote 7 is made by degradation of Amioca, in this case, the former also has a lower molecular weight.

It is seen that for a given probe the zero-concentration diffusion coefficient D_0 is insensitive to the matrix starch, despite the differences in their overall molecular weights. However, the data for the concentration dependence of the relative diffusion coefficient show that the two lower molecular weight polymers—Stakote 7 and 2×10^6 dextran—retard the probe to a greater extent (on a weight basis) than the two higher molecular weight, native waxy starches. This is counterintuitive but can be rationalized as follows.

Semicrystalline amylopectin is a very compact molecule, with extensive branching and may have an oblate ellipsoidal shape in aqueous solutions.[20] The chain length distribution of Stakote 7 and dextran suggest that they would be much more spherical

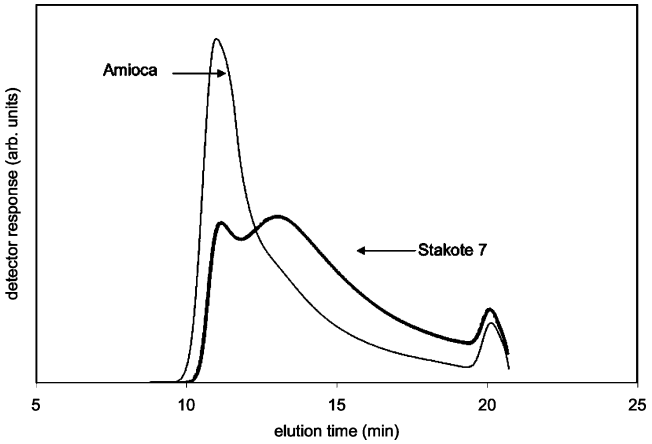

Figure 7. Size-exclusion chromatogram showing the response of the refractive index detector during elution of Amioca waxy corn starch and its partially chemically degraded derivative, Stakote 7. The decrease in high molecular weight chains (short retention time) and increase in low molecular weight chains (longer retention times) are apparent.

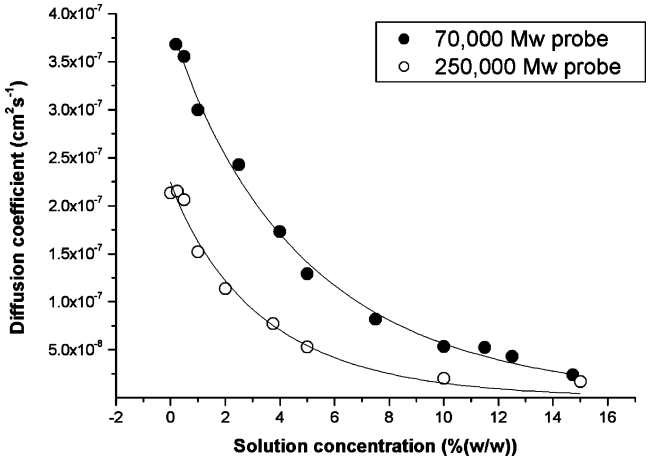

Figure 8. Variation in the diffusion coefficient of two different molecular weight FITC-Dextran probes as a function of 2×10^6 $\bar{M}_w$ dextran matrix concentration. Solid lines are the stretched exponential fits to the data.

and less compact in aqueous solution.[20] It is reasonable to suppose that gels made of less compact molecules would retard the probe to a greater extent than would gels of flat or oblate shapes. The relative diffusion data suggest that molecular weight is not the only factor governing diffusion: there may well be a significant part played by the shape and conformation of the molecules.

There is little to distinguish the diffusion behavior of Amioca and Shimizu starches, with any variations in molecular weight or architecture having little effect. This is analogous to saying that diffusion here is only a factor of concentration (increasing which serves to tighten the mesh through which molecules must diffuse), with little dependence on molecular weight or specific architecture.[21]

Fitting Diffusion Coefficients to a Model. There are predictive models for the behavior of *linear* monodisperse polymers in the entangled, semidilute regime[21] but none for branched polymers, such as those used, although some efforts have been made in this direction.[22,23] In their place, empirical relationships have been derived from studies of spherical probe diffusion in polymeric solutions, which, although based on a number of different physical models, all lead to formulas where the reduced diffusion coefficient (D/D_0) is a stretched exponential function of the polymer matrix concentration.[24−26] Although there are reservations about using such a model, its general applicability and utility have been demonstrated, for example in the cited references.

In its most common representation, that of Phillies,[26] the stretched exponential scaling equation for the diffusion coefficient D of a tracer probe at concentration c takes the form

$$D = D_0 \exp(-\beta c^{\upsilon}) \tag{5}$$

where β and υ are empirical constants, with β a function of the probe size and its interaction with the polymeric matrix, and υ is attributed to the solution properties of the polymer and falls between 0.5 and 1 for several systems investigated. A further prediction of the hydrodynamic model of tracer diffusion of Phillies relates β to the molecular weights of the polymer matrix (M_{polymer}) and the probe (M_{probe})

$$\beta \propto \sqrt{M_{\text{polymer}} M_{\text{probe}}} \tag{6}$$

A number of studies have used the stretched exponential to model diffusion coefficients obtained using FRAP as a function of solution concentration,[9,13,22,23] and eq 6 has been shown to be very effective at fitting the behavior across the whole concentration range with only a single set of parameters. This is also found to be the case with the current data, despite the complex structure of the matrix polymers, most notably their branched and polydisperse nature. Figure 8 shows the stretched exponential fit to the data for the diffusion of the dextran probes in solutions of 2×10^6 $\bar{M}_w$ dextran; this is typical of the fitting for all of the starches used here. Table 1 gives the fitted values of the parameters D_0, β, and υ for the three starches investigated, with the 7.0×10^4 $\bar{M}_w$ FITC-dextran probe, and for the two different probes in the dextran matrix.

It can be seen from the values of υ that for the case of these starch samples the stretched exponential simplifies to $D = D_0 e^{-\beta c}$. Mobility of the FITC-dextran probe is restricted to a greater extent as the matrix polymer concentration increases, but mobility is not prevented and does not undergo any step-change in behavior as concentration increases, despite there having to be quite extensive interpenetration and possible entanglement of starch polymer chains at concentrations greater than 10 times the overlap concentration. This mobility is aided by the flexibility of the dextran probe, as it is able to more easily pass through a dense matrix than is a rigid colloidal probe, such as latex spheres.[9] Also evident is the similarity of all of the values for β for these samples, to within the limits of the uncertainty. This is as expected, as we are using the same probe molecule within solutions with polymers with molecular weights of the same order of magnitude that have the same polymeric units and hence similar solvent−polymer interactions.

The theory of Phillies can be tested by examining the prediction of the combined molecular weight dependence of the parameter β, as given in eq 6. For the two different molecular weight short-branched FITC-dextran probes in the same polymeric matrix, the ratio of the two values of the value of β is indeed proportional to the square root of molecular weight: the ratio of the values of $\beta \sim 0.23/0.43 = 0.53$ is the same (to two significant figures) as the square root of the ratio of their molecular weights. The same simple treatment however fails to determine the molecular weight of the matrix starch polymers from comparison of the β values from dextran and starch solutions due to the different nature of the two polymers:

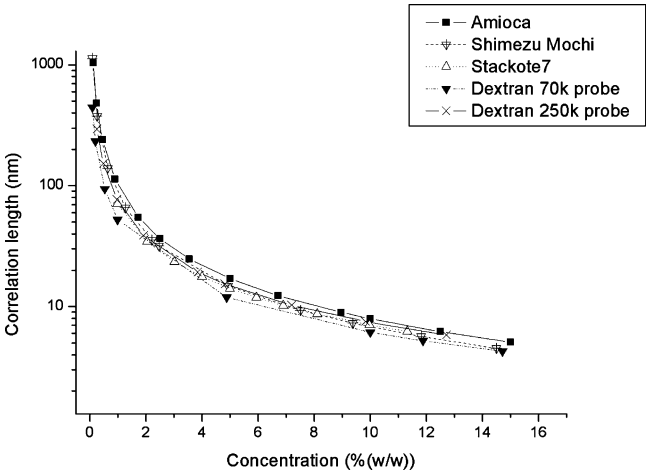

Figure 9. Correlation length as a function of solution concentration, as determined from the parameters derived from the fitting of the stretched exponential (eq 5) to full recovery curves. The data for dextran (2×10^6 $\bar{M}_w$) with the 2.5×10^5 $\bar{M}_w$ FITC-Dextran probe is that obtained using the parameters from a normalized (D/D_0) fit.

dextran is long-chained with short branches whereas amylopectin has a highly branched and complex architecture.

Comparison of fitting parameters from different starches, or more particularly the same starch at various stages of hydrolysis, may prove more accessible to analysis in this manner. The starches used in this study are all of comparable molecular weight and would be expected to produce values on the same order of magnitude, to within the limits of the uncertainty.

The stretched exponential fitting of the full dependence of diffusion coefficients on concentration can be interpreted to yield the variation of the mesh size or correlation length, ξ, of the polymeric solution with increasing concentration. The network is transient due to the temporary nature of each chain−chain association or entanglement and thus ξ is an average of a distribution of apparent mesh sizes. The mesh size is given by[18]

$$\xi = \frac{d}{\beta} c^{-v} \tag{7}$$

where d is the diameter of the probe molecule. The resulting concentration dependence of ξ is shown in Figure 9.

It can be seen that the variation in correlation length with increasing starch concentration for each of the starch varieties is very similar, due to the self-similarity of the amylopectin molecules that constitute the majority of the polymeric component of each of these varieties. At the lowest concentrations, the correlation length is very large, as the individual chains are well separated in space and there is no overlap. At the highest concentrations investigated, the correlation length drops to between 4 and 5.5 nm for all samples. At these high concentrations, from about 9% (w/w) and above, the mesh size of the polymer solution has dropped to below the hydrodynamic radius of the probe molecules ($R > \xi$) and the probe can be thought of as encountering a continuous starch matrix. Variations in the value of correlation length with starch origin, degree of hydrolysis, degree of branching, etc., and the relation of the correlation length to the size and nature of the diffusing species, could prove very important for food processing properties of starch solutions and pastes. The probe molecules used in this study are flexible polymer chains that are capable of multiple modes of diffusion. We would expect to observe quite different behavior if we were to study the behavior of rigid probes, such as latex spheres.

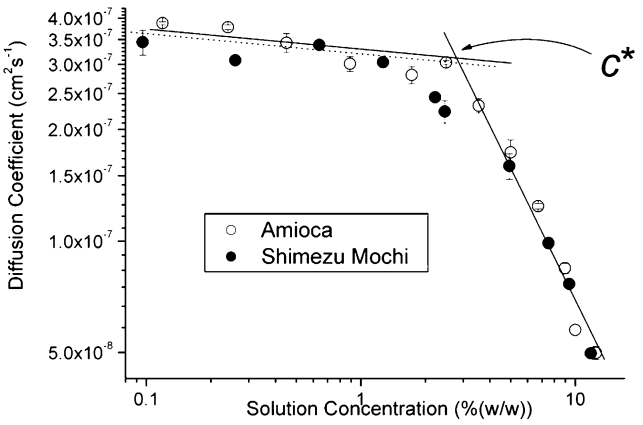

Figure 10. Some of the data of Figure 5 plotted double-logarithmically, showing a possible method of inferring values of the critical overlap concentration c^*.

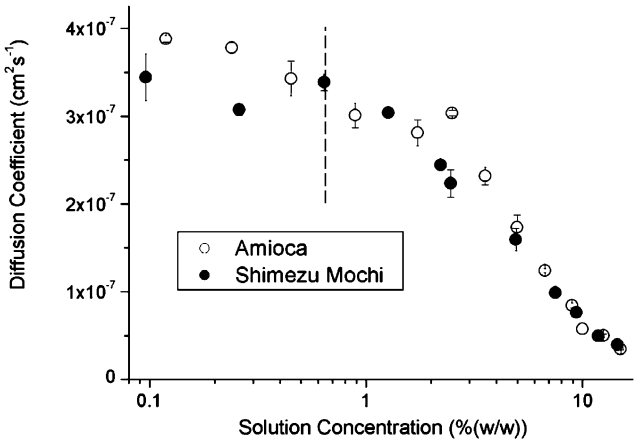

Figure 11. Data of Figure 10 as a semilog plot, showing alternative value of c^* (dashed line).

Critical Overlap Concentration. A parameter that is frequently used to characterize polymer solution behavior is the critical overlap concentration, c^*: the concentration that marks the transition from the dilute to the semidilute solution regime due to the incipient overlap and entanglement of separate polymer chains. It is given by

$$c^* = \frac{3M}{4\pi N_A \langle s^2 \rangle^{3/2}} \tag{8}$$

where N_A is the Avogadro constant, M is the molecular weight, and $\langle s^2 \rangle^{1/2}$ is the radius of gyration. For Amioca starch, $c^* =$ 0.66% (w/w), from eq 8 and literature values of molecular weight, M (2.54×10^9), and $\langle s^2 \rangle^{1/2}$ (250 nm).

It has been suggested[22,27] that the value of c^* can be inferred from a sharp change in behavior of the diffusion coefficient with increasing matrix polymer concentration. Figure 10 shows a double-logarithmic representation of diffusion coefficient vs concentration data for Amioca starch, and marked on this plot is the value of c^* obtained by the intersection of the lines from a linear fit to the two extremes. The diffusion coefficient decreases as the matrix polymer concentration increases with an apparent rapid change at a particular concentration (∼3% in this case), a qualitative behavior seen in many other systems. Taking the point of transition as being the first significant deviation from the zero concentration diffusion coefficient brings the apparent c^* value down to below 1% (w/w), as can be seen from the semilog plot shown in Figure 11. This behavior might suggest that there is a change in the mode of diffusion as

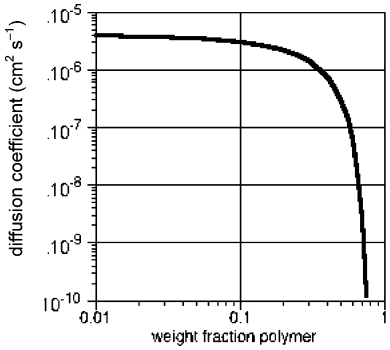

Figure 12. Diffusion coefficient of hydroxyethyl methacrylate in a solution of its polymer in water at 25 °C as a function of weight-fraction polymer calculated using free-volume parameters fitted to experimental data,[35] treated in the same way as the data of Figure 10.

concentration increases, and is sometimes attributed, particularly when interpreting self-diffusion data, to the continuous change from Rouse to reptation dynamics.[28] However, the scaling theories that would characterize such behavior were developed for monodisperse self-diffusion of linear polymers, where the probe and polymer molecular weights are at least comparable. This is not the case for the kind of probe diffusion performed here or in other studies using FRAP, where the probes are much smaller than the polymers forming the matrix, which are also highly branched and polydisperse.

All of these values of c^* are similar but certainly do not lie within each other's experimental uncertainties. The values, ~1% w/w, are consistent with the overlap concentration obtained by Ring et al.[29] from viscometric studies of Amioca starch. This value contrasts with other work[30] that cites a c^* value of 10% (w/w) for Amioca starch, although of course this depends on the specific degree of hydrolysis of the starch and its resulting molecular weight. It is clear in the case of probe diffusion, as opposed to direct measurements of viscosity, there is no single point which we can designate as the domain overlap concentration. Much care needs to be taken when considering any graphical determination of changes in diffusion behavior.

In addition to the uncertainty regarding the specific location of the overlap concentration in a probe diffusion experiment, there is disagreement as to the actual physical significance of these concepts when one is dealing with diffusion behavior. Some authors, such as Phillies,[31−34] suggest that polymer−polymer interactions are dominated by hydrodynamic forces rather than entanglement or topological effects. This viewpoint is supported by the present data, as shown in Figure 8, indicating that rheological behavior for a given probe across the whole concentration range of the polymeric solution can be modeled using one set of parameters, without a change in behavior at some arbitrary point at which overlap or entanglements are predicted to occur. As another extreme example showing the care that needs to be taken with the inference of a value of c^* from a log−log plot is shown in Figure 12. This shows the same type of log/log plot for diffusion coefficient data of a water-soluble monomer, hydroxyethyl methacrylate, diffusing in its polymer dissolved in water, obtained using pulsed-field gradient NMR.[35] The plot shows the line obtained by fitting the experimental data by free-volume theory,[36] where there is no physical reference at all to an overlap concentration. This double-logarithmic plot is qualitatively similar to that of Figure 10, yet this was calculated using a model without any reference to an overlap concentration or analogous concept. This extreme example, and the disagreement with the two methods for estimating c^* for the starch system, show that caution must be taken when making inferences from values of c^* found using double-log plots.

Effects of Ionic Strength on Probe Dimensions. It is also interesting to see to what extent it is possible to vary the properties of the probe within a system of interest by variation of ionic strength. This was carried out here by performing FRAP in sodium chloride solutions of varying concentration, from 0.8 to 6.13 M (saturation) within the probe-containing solution. The free diffusion of the 7.0×10^4 and 2.5×10^5 $\bar{M}_w$ FITC-dextran probes was examined as well as the behavior of the 7.0×10^4 $\bar{M}_w$ probe in a 2% (w/w) Shimizu Mochi starch solution. It can be seen from the resulting data, shown in Figure 13, that there is an approximately linear decrease in diffusion coefficient with the increase in ionic strength brought about by the addition of sodium chloride to both the free probe molecules and the FITC-dextran probe in the 2% starch solution. Values of the parameters from the linear fits to each of the three data sets are shown in Table 2. The decrease in diffusion coefficient is brought about by the increase in size of the probe dextran molecules, which are highly branched but essentially spherical coil polymers. This is supported by the work of Chiou et al.,[37] which showed (using photon correlation spectroscopy) that the size of many (but not all) branched starches increases significantly over the range of [NaCl] used here; the changes in the PCS distributions showed that these increases were due to chain expansion, not interactions between starch chains. The increase in ionic strength serves to expand the chains and increase the effective diameter of the dextran molecules in solution, leading to greater frictional retardation of the chains as they pass through the aqueous solution.

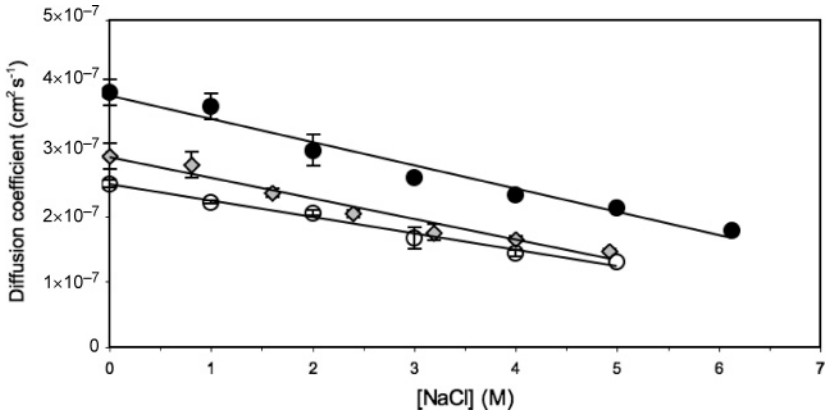

Figure 13. Diffusion coefficient of 7.0×10^4 $\bar{M}_w$ and 2.5×10^5 $\bar{M}_w$ FITC-dextran probes in both free solution (filled and open circles, respectively) and 7.0×10^4 FITC-dextran probe mixed with 2% (w/w) Shimizu Mochi waxy rice starch (diamonds), as a function of sodium chloride concentration.

Table 2. Parameters from Linear Fits to the Variation of Diffusion Coefficient with Increasing Ionic Strength Data Shown in Figure 13

	slope/cm^2s^{-1} M^{-1}	intercept/cm^2s^{-1}
free 7.0×10^4 $\bar{M}_w$ FITC-dextran probe	$-3.6 \pm 0.4 \times 10^{-8}$	$3.9 \pm 0.2 \times 10^{-7}$
2% Shimizu Mochi starch + 7.0×10^4 M_w FITC-dextran probe	$-3.2 \pm 0.5 \times 10^{-8}$	$2.9 \pm 0.2 \times 10^{-7}$
free 2.5×10^5 $\bar{M}_w$ FITC-dextran probe	$-2.2 \pm 0.2 \times 10^{-8}$	$2.4 \pm 0.1 \times 10^{-7}$

Based on earlier work on starch gelatinization,[38] which showed that salt assists in forming an ordered structure within water and also interacts with the hydroxyl groups on the glucose units, it seems reasonable to assume that increasing salt concentrations enhances the interactions between water and the hydrophilic polymer, whether starch or dextran, and hence leads to chain expansion.

When we compare the decrease in diffusion coefficient for the free 7.0×10^4 $\bar{M}_w$ probes and for the starch solution containing the 7.0×10^4 $\bar{M}_w$ probe, it can be seen that the slope of the decrease is the same in both cases, with the presence of the starch serving only to shift the whole curve to lower levels, due to the increased viscosity produced in the system by the starch polymer solution. This is very revealing as it shows that, at least in the semidilute regime, where there is already overlap (and possible entanglement) of polymer chains (and presumably also in very dilute solution, where polymer chains are well separated), probe diffusion behavior is affected only, or at least predominantly, by the size of the tracer probe molecules, with the starch chains expanding little or not at all in this regime and with these salt concentrations. Again, this is supported by Chiou et al.,[37] who showed that the diameter of starch chains from Shimizu Mochi starch do not change significantly upon increasing the concentration of NaCl until a concentration of around 5 M is reached, at which point an increase in size is observed. The present data for the mixed starch-probe system is all at 5 M or below, in the region where no significant expansion of the Shimizu Mochi starch chains is expected. Chiou et al. also put forward the suggestion that branched starches composed of longer glucan chains are expanded to a greater extent than those composed of more short chains. This is consistent with the present observations, with the long linear dextran, with multiple short branches, being much more expandable than the multiple clusters of short chains that make up a hyperbranched starch molecule.

If the starch chains were affected in the same way as the dextran chains, then we would expect to observe a significant divergence in the diffusion coefficient vs salt concentration plots of free probe and probe + starch, as the expansion of both the probe and the matrix molecules serve to slow the diffusion of the probe molecules. This is most likely due to the highly branched and compact nature of the amylopectin chains being far less susceptible to swelling and expansion, especially in the semidilute regime, than the more open and unencumbered dextran chains. The complex nature of branching within the amylopectin component of starch, with multiple clusters of short branches, connected via nonrandomly positioned branch points, also acts to limit the degree to which the starch chains can expand. Despite this finding here with one starch, Shimizu Mochi, it is clear that different starch varieties may behave differently, as is shown by the work of Chiou et al. It seems that the ratio of long to short chains and the extent and distribution of branch points may be the main determinants of the degree of expansion and swelling.

It is also possible that the starch chains *do* expand significantly in the presence of the salt but that the effective mesh size of the solution is not reduced to any great extent, due to the now more open and expanded chain structures. The increase in the size of the probe slows its diffusion, as we would expect, but the increase in the average size of a starch chain does not serve to slow the probe further as there is still sufficient space within the solution for the probe to pass. A different result may be observed in more concentrated and densely packed starch solutions.

This work contrasts with a previous study of the effects of sodium chloride on probe diffusion in hyaluronan solutions,[22] in which NaCl acted as an electrostatic shield, resulting in contraction of the polyanions and accompanying increase in the diffusion coefficient of the FITC-dextran probe. The NaCl concentration was also so low (<0.5 M) as to not impact upon the size of the polymeric probe.

Conclusions

This study illustrates the power and potential of fluorescence recovery after photobleaching combined with confocal microscopy to probe the structure and dynamics of starch solutions, by determining the diffusion coefficient of a tracer probe molecule within a starch-based matrix. This work has laid the groundwork for future studies of molecular architecture and its effects on mobility and for investigation of the effects of variations in branching, molecular weight and relative polymer composition, whether naturally occurring or produced by enzymatic or chemical modification.

The diffusion behavior of a probe molecule is dependent upon the size R of the probe, relative to the average mesh size, or correlation length, ξ, of the matrix polymer solution, as well as on the fractal dimensions of the probe.[9,10] Probes that are small compared to the mesh size will exhibit different behavior to those where $R > \xi$ and flexible polymeric probes (such as dextrans) experience less hindrance to diffusion than colloidal, inflexible probes (such as polystyrene latex spheres) in the semidilute regime. This leads to the conclusion that parameters determined from tracer-probe FRAP studies will vary, depending on the size and nature (flexible polymeric vs rigid colloidal) of the probe used. This, combined with specific enzyme action and chemical means, provides us with a potentially powerful means to examine the influence of such factors as degree of branching, solvent quality and phase separation on the local dynamics of starch systems.

The dilute solution behavior of starch is also of interest due to the relative lack of information about this area and the controversy that still exists about some of the fundamental parameters that define starch behavior. The major causes of complication are: the complex nonrandomly branched structure of the major polymeric component of starch, amylopectin; the polydispersity of starch structure (i.e., a given sample contains chains with a wide range of molecular weights, branching frequencies, etc.); the great biological variety of starch, that depends not only on botanical origin, but also on growing conditions (temperature, light exposure etc.) and the geographical growth region of the starch;[39] and the wide variety of experimental techniques that have been used to study starch systems.

The diffusion characteristics of starch are of importance when we come to consider the transport of small molecules within

starch systems and the accessibility and ease of diffusion of enzymes. The availability of starch to enzymes and the rate at which the enzymes can penetrate concentrated starch solutions and pastes could be a key factor in determining the ease and rate of starch digestion. This could be of importance in understanding some of the key features of the texture of processed foods in which starch is an ingredient of the matrix. Other potential applications are to follow the development of and map compositional inhomogeneities, brought about by processing conditions or more fundamental phase separation, agglomeration or gelation, and the diffusion and transport of small molecules through starch pastes and gels, as a model of the transport of flavor compounds, additives etc.

These preliminary studies of the probing of starch solutions and pastes with FRAP and tracer probe diffusion also opens up another potentially useful area of investigation. Probe diffusion coefficients, including dependence on ionic strength, is also a means of characterizing the complex architecture of branched polymers, especially amylopectin. Combining tailored breeding and enzymatic modification of complex structural natural polymers with accurate and sensitive probes of diffusion such as FRAP tracer probe diffusion holds great potential for furthering our knowledge of the full range of polymer structure−property relationships.

Acknowledgment. We thank the Rural Industries Research and Development Council (RIRDC), Australia, for the funding to support this work. We thank. Drs Ewan Sprong and Hank de Bruyn for the SEC data of Amioca and Stakote 7 starches. We also thank Ellie Kable, Laboratory Manager of the Electron Microscopy Unit at the University of Sydney, for technical assistance with FRAP protocols and the use of the confocal microscope and Gavin Rea for early work in this area. The Key Centre for Polymer Colloids was established and supported by the Australian Research Council's Research Centres program.

References and Notes

(1) Burke, M. D.; Park, J. O.; Srinivasarao, M.; Khan, S. A. *Macromolecules* **2000**, *33*, 7500−7507.
(2) Stavreva, D. A.; McNally, J. G. *Methods Enzymol. Pt. A* **2004**, *375*, 443−455.
(3) Rabut, G.; Ellenberg, J. *J. Microsc.-Oxford* **2004**, *216*, 131−137.
(4) van Drogen, F.; Peter, M. *Methods Mol. Biol.* **2004**, 284, 287−306.
(5) Huang, W.; Frick, T.; Landry, M.; Lee, J.; Lodge, T.; Tirrell, M. *AIChE J.* **1987**, *33*, 573.
(6) Kogelnik, H. *Bell Syst. Technol. J.* **1969**, *48*, 2909.
(7) Tonge, M. P.; Stubbs, J. M.; Sundberg, D. C.; Gilbert, R. G. *Polymer* **2000**, *41*, 3659−3670.
(8) Axelrod, D.; Koppel, D. E.; Schlessinger, J.; Elson, E.; Webb, W. W. *Biophys. J.* **1976**, *16*, 1055−1069.
(9) Cheng, Y.; Prud'homme, R. K.; Thomas, J. L. *Macromolecules* **2002**, *35*, 8111−8121.
(10) Pluen, A.; Netti, P. A.; Jain, R. K.; Berk, D. A. *Biophys. J.* **1999**, *77*, 542−552.
(11) Chiou, H.; Martin, M.; Fitzgerald, M. A. *Starch/Staerke* **2002**, *54*, 415−420.
(12) Blonk, J. C. G.; Don, A.; van Aalst, H.; Birmingham, J. J. *J. Microsc.* **1993**, *169*, 363−374.
(13) De Smedt, S. C.; Meyvis, T. K. L.; Demeester, J.; Van Oostveldt, P.; Blonk, J. C. G.; Hennink, W. E. *Macromolecules* **1997**, *30*, 4863−4870.
(14) Braeckmans, K.; Peeters, L.; Sanders, N. N.; De Smedt, S. C.; Demeester, J. *Biophys. J.* **2003**, *85*, 2240−2252.
(15) Furukawa, R.; Arauz-Lara, J. L.; Ware, B. R. *Macromolecules* **1991**, *24*, 599−605.
(16) Callaghan, P. T.; Pinder, D. N. *Macromolecules* **1983**, *16*, 968−973.
(17) Callaghan, P. T.; Lelievre, J. *Anal. Chim. Acta* **1986**, *189*, 145−166.
(18) De Smedt, S. C.; Lauwers, A.; Demeester, J.; Engelborghs, Y.; De Mey, G.; Du, M. *Macromolecules* **1994**, *27*, 141−146.
(19) Flory, P. J. *Principles of Polymer Chemistry*; Cornell University Press: Ithaca, NY, 1953.
(20) Caldwell, R. A.; Matheson, N. K. *Carbohydr. Polym.* **2003**, *54*, 201−213.
(21) de Gennes, P.-G. *Scaling Concepts in Polymer Physics*; Cornell University Press: Ithaca, NY, 1979.
(22) Gribbon, P.; Hardingham, T. E. *Biophys. J.* **1998**, *75*, 1032−1039.
(23) Gribbon, P.; Heng, B. C.; Hardingham, T. E. *Biophys. J.* **1999**, *77*, 2210−2216.
(24) Cukier, R. I. *Macromolecules* **1984**, *17*, 252−255.
(25) Altenberger, A. R.; Tirrell, M. *J. Chem. Phys.* **1984**, *80*, 2208−2213.
(26) Phillies, G. D. J.; Gong, J.; Li, L.; Rau, A.; Zhang, K.; Yu, L. P.; Rollings, J. *J. Phys. Chem.* **1989**, *93*, 6219−6223.
(27) Han, J. A.; Lim, H.; Lim, S. T. *Starch/Staerke* **2005**, *57*, 262−267.
(28) Nydén, M.; Söderman, O. *Macromolecules* **1998**, *31*, 4990−5002.
(29) Ring, S. G.; Colonna, P.; I'Anson, K. J.; Kalichevsky, M. T.; Miles, M. J.; Morris, V. J.; Orford, P. D. *Carbohydr. Res.* **1987**, *162*, 277−293.
(30) Durrani, C. M.; Donald, A. M. *Carbohydr. Polym.* **2000**, *41*, 207−217.
(31) Phillies, G. D. J.; Malone, C.; Ullmann, K.; Ullmann, G. S.; Rollings, J.; Yu, L. P. *Macromolecules* **1987**, *20*, 2280−2289.
(32) Phillies, G. D. J.; Peczak, P. *Macromolecules* **1988**, *21*, 214−220.
(33) Phillies, G. D. J.; Kirkitelos, P. C. *J. Polym. Sci., Part B: Polym. Phys.* **1993**, *31*, 1785.
(34) Phillies, G. D. J.; Streletzky, K. A. *Recent Res. Devel. Phys. Chem.* **2001**, *5*, 269−285.
(35) Strauch, J.; McDonald, J.; Chapman, B. E.; Kuchel, P. W.; Hawkett, B. S.; Roberts, G. E.; Tonge, M. P.; Gilbert, R. G. *J. Polym. Sci. A Polym. Chem. Ed.* **2003**, *41*, 2491−2501.
(36) Vrentas, J. S.; Vrentas, C. M. *Eur. Polym. J.* **1998**, *34*, 797−803.
(37) Chiou, H.; Fellows, C. M.; Gilbert, R. G.; Fitzgerald, M. A. *Carbohydr. Polym.* **2005**, *61*, 61−71.
(38) Jane, J. L. *Starch* **1993**, *45*, 161−166.
(39) Banks, W.; Greenwood, C. T. *Starch and its components*; Edinborough University Press: Edinborough, 1975.

BM0507711